

Frankenstein Optimizer: Harnessing the Potential by Revisiting Optimization Tricks

Chia-Wei Hsu¹ Nien-Ti Tsou² Yu-Cheng Chen³ Yang Jeong Park⁴ Ju Li^{1,4}

¹Department of Materials Science and Engineering, Massachusetts Institute of Technology, Cambridge, MA 02139

²Department of Materials Science and Engineering, National Yang Ming Chiao Tung University, Taiwan

³Hon Hai Research Institute, Taipei, Taiwan

⁴Department of Nuclear Science and Engineering, Massachusetts Institute of Technology, Cambridge, MA 02139

Correspondence to: Yang Jeong Park <parkyj@mit.edu>, Ju Li <liju@mit.edu>.

Abstract

Gradient-based optimization drives the unprecedented performance of modern deep neural network models across diverse applications. Adaptive algorithms have accelerated neural network training due to their rapid convergence rates; however, they struggle to find “flat minima” reliably, resulting in suboptimal generalization compared to stochastic gradient descent (SGD). By revisiting various adaptive algorithms’ mechanisms, we propose the Frankenstein optimizer, which combines their advantages. The proposed Frankenstein dynamically adjusts first- and second-momentum coefficients according to the optimizer’s current state to directly maintain consistent learning dynamics and immediately reflect sudden gradient changes. Extensive experiments across several research domains such as computer vision, natural language processing, few-shot learning, and scientific simulations show that Frankenstein surpasses existing adaptive algorithms and SGD empirically regarding convergence speed and generalization performance. Furthermore, this research deepens our understanding of adaptive algorithms through centered kernel alignment analysis and loss landscape visualization during the learning process. Code is available at https://github.com/acctouhou/Frankenstein_optimizer

1. Introduction

In recent years, neural networks (NNs) have become increasingly prevalent in various fields, driving the widespread adoption of gradient-based optimization methods in science and engineering. This increased usage has led to studies enhancing optimizers to achieve faster convergence and better results with limited computational resources. Among

these optimizers, Adam([Kingma, 2014](#)) has emerged as the most prominent, often serving as the default setting in deep learning tasks. However, many studies have highlighted that Adam-like optimizers do not necessarily achieve superior generalization([Zhou et al., 2020](#); [Lyu & Li, 2019](#)), with simple experiments([Wilson et al., 2017](#)) demonstrating this issue. As a result, the debate between Adam and stochastic gradient descent (SGD) has persisted within the deep learning community.

The rapid growth in the parameter size of deep learning models has magnified the importance of adaptive optimizers despite their known limitations ([Villalobos et al., 2022](#)). Current state-of-the-art large language models (LLMs), such as Nemotron-4 with 340 billion parameters ([Adler et al., 2024](#)), LLaMA 3.1 with 405 billion parameters([Dubey et al., 2024](#)) and DeepSeek-V3 with 671 billion parameters ([Liu et al., 2024](#)), exemplify the growing scale of modern architectures. Considering the computational cost for training GPT-3 with 175 billion parameters ([Brown et al., 2020](#)) which amounts to \$4.6 million, it is obvious that the efficiency of optimization algorithms directly impacts AI economics.

Adam or its variants have been actively developed to design faster optimizers. For example, AdaBelief([Zhuang et al., 2020](#)) demonstrates its superiority in addressing deep valley problems by simultaneously considering both adaptive terms and momentum. Similarly, Sophia optimizer([Liu et al., 2023](#)) showcases its ability to manage risks in the update process by correcting the Hessian, ensuring its stability, and yielding promising results in large models like LLMs. However, the adaptive nature during optimization remains underexplored, leaving room for further improvement.

To further explore these adaptive adjustments and the potential for improvement, we propose a new optimizer, “Frankenstein,” developed on the techniques used by previous gradient-based adaptive optimizers, while incorporating our three key innovations:

- **1) Adaptive momentum coefficients β :** Unlike previous optimizers that employ a fixed momentum coefficient, our approach dynamically adjusts the momentum based on the current state and learning rate schedule. This design enhances the adaptability of the optimization process, enabling more efficient convergence across diverse training scenarios.

- **2) Relaxation strategy for second momentum v_t :** Along with adjusting the second momentum, we propose a novel relaxation strategy that balances the maximum recorded value, as utilized in AMSGrad variants (Reddi et al., 2019), with conventional unconstrained exponential moving average methods. This approach accelerates optimization while mitigating convergence risks, resulting in significant improvements in solving adaptive problems.

- **3) Acceleration factor ξ :** For fast and accurate convergence, we designed an acceleration factor that comprehensively evaluates the system’s gradient magnitude and degree of belief, as well as its proximity to convergence. It determines how much the gradient is reflected in the parameter update.

To briefly demonstrate the effect of those design principles, we visualize optimization process of various existing adaptive algorithms and Frankenstein on a loss function, as shown in Fig.1. In scenarios with larger gradients, our method achieves acceleration up to 1.6 times the standard learning rate. However, as convergence approaches, updates rely primarily on the second momentum term, which decays more rapidly, making the nonlinear misalignment factor P the primary factor driving acceleration. This produces two distinct peaks in the normalized adaptive factor. The adaptive factor is defined as any value applied to momentum or gradients during the position update that controls the learning rate. The adaptive factor throughout the entire learning process contributes to understanding the optimizer’s preferences and behavior. This switching mechanism also achieves robust convergence in plateaued landscapes(McClean et al., 2018), which is a significant issue for quantum NN training. ξ will ultimately revert to a value of 1, which is the non-accelerated state, due to the vanishing gradient and the convergence of nonlinear P factor.

In the remainder of this paper, we provide a more detailed explanation of the algorithm 1 and validate its superiority through experiments across various applications. Various visualization analyses during the learning process were conducted to gain a deeper understanding of the algorithm’s adaptability.

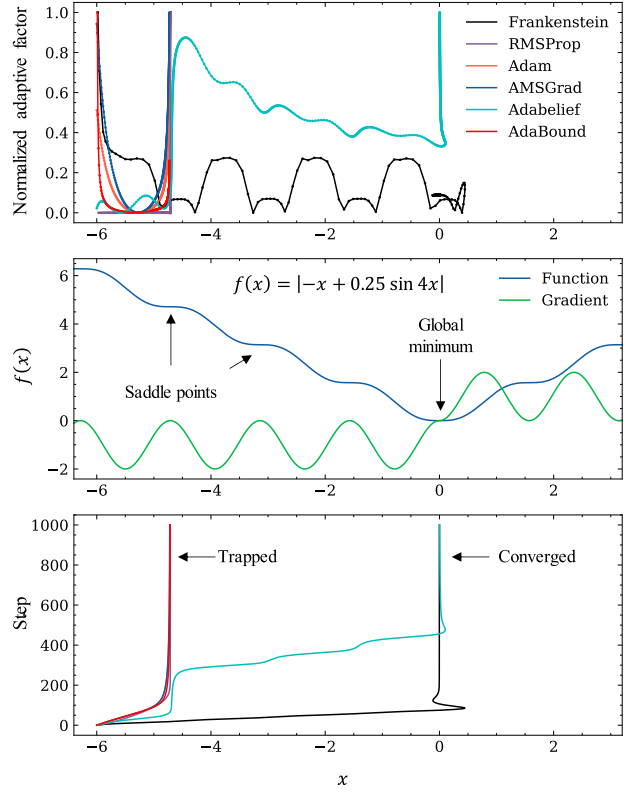


Figure 1. From top to bottom: (1) Adaptive factor for each optimizer during the optimization process of $f(x)$; (2) Function $f(x)$ and its corresponding gradient; (3) Historical trajectories of each optimizer as a function of optimization steps.

2. Algorithm

2.1. Adaptive first momentum coefficient β

Adjusting the learning rate throughout NN training is a common strategy to improve model performance. Research indicates(Smith, 2017; Wu et al., 2018; Goyal et al., 2019) that there should be a consistent “noise scale” across batch size, learning rate, and momentum. Therefore, our proposed algorithm also adapts the momentum coefficient based on the current learning rate. In Verlet integration, Δx is affected by the current momentum, gradient, and learning rate, as illustrated in Equation 1. Let α represent the learning rate, m_t represent the first-order momentum, g_t represent the gradient, and θ represent the learning parameter.

$$\theta_{t+1} = \theta_t + m_t \alpha + \frac{1}{2} g_t \alpha^2 \quad (1)$$

If the training process enters a stable phase where the gradient remains relatively constant and the momentum closely matches the gradient, the momentum coefficient should be maintained as specified in Equation 2; otherwise, this bal-

ance could be disrupted.

$$(1 - \beta)m_t \approx \frac{1}{2}g_t\alpha^2 \quad (2)$$

To maintain training consistency, the decay rate caused by momentum and the momentum coefficient should correspond to the gradient and the learning rate; otherwise, using a learning rate decay strategy might lead to overly rapid convergence, requiring additional iterations to achieve the optimal convergence point. Based on this insight, we propose a momentum coefficient adjustment strategy, detailed in Equation 3. This formula reflects common configurations, where training from scratch uses $\alpha = 10^{-3}$ and $\beta = 0.9$, while fine-tuning adopts $\alpha = 2 \times 10^{-4}$ and $\beta = 0.9$. In our algorithm, each time the learning rate changes, a new optimal β^* is calculated based on the corresponding learning rate instead of using a fixed β .

$$\beta^* = 1 - (1 - \beta)\sqrt{\frac{\alpha}{10^{-3}}} \quad (3)$$

It's worth noting that other algorithms update momentum by applying a fixed-coefficient moving average, which retains information from multiple previous steps during iterations and smooths the trajectory. This approach takes several steps to approximate the ideal state. In contrast, our Frankenstein can directly maintain consistent learning dynamics. In other words, it isn't forced to converge due to changes in the learning rate; instead, it decides whether to converge based on the actual gradient conditions (with the final momentum coefficient still remaining < 1).

Here, we define the nonlinear misalignment factor (P), which indicates a misalignment between the past momentum m_{t-1} and current gradient g_t . P takes a value between 0 and 1, and it becomes smaller when the two vectors are well-aligned in the same direction, while it becomes larger when they are aligned in opposite directions.

$$P \leftarrow \cos^{-1}(\tanh(m_{t-1} \odot g_t)) / \pi \quad (4)$$

Additionally, the we propose another parameter ρ to adjust the momentum coefficient.

$$\rho \leftarrow \log(e^1 + \sqrt{x_t} + 0.5 - P) \quad (5)$$

where x_t refers the summation of squared gradient g_t^2 and a small constant ϵ . The ρ parameter controls whether the momentum coefficient should increase based on the difference between the current system state and the ideal convergence state. The coefficient is influenced by two conditions: (1) whether the squared gradient approaches zero and (2) whether the P factor approaches 0.5. As these conditions near the convergence state, the momentum coefficient will

gradually decrease to the default value of β , effectively rendering it inactive.

Notably, the momentum coefficient can be adjusted to zero if the product of the momentum direction and the gradient is highly negative. This mechanism is inspired by the FIRE algorithm(Guénolé et al., 2020), where a large directional discrepancy may indicate that the step size is too large, causing a lack of convergence. Therefore, this feature includes reinitializing the momentum or reversing its direction when necessary.

2.2. Second momentum v_t update with dynamic EMA

The update rules for second momentum v_t enable various strategies to achieve optimizers' adaptivity. The general process is outlined in the formula below.

$$g_t \leftarrow \nabla_\theta f_t(\theta_{t-1}) \quad (6)$$

$$v_t \leftarrow V(v_{t-1}, g_t, \beta, \dots) \quad (7)$$

$$\theta_{t+1} \leftarrow U(\theta_t, v_t, \alpha, \dots) \quad (8)$$

where V represents a momentum update function and U represents a parameter update function.

Starting with the basic RMSProp strategy, which applies a simple Exponential Moving Average (EMA) to the squared gradients, several adaptations have been developed (Appendix C). These methods depends on a fixed β_2 parameter throughout the training process. In contrast, this work proposes a strategy that also relies on squared gradients as its foundation but applies an EMA coefficient that adapts based on both current and historical states. This coefficient is determined by whether the P factor approaches 0.5 and the ratio of the current to past squared gradients. The following paragraphs explain the motivations for this adjustment.

These Adam-like optimizers employ adaptive methods with second-order momentum, using a higher momentum coefficient for EMA compared to first-order momentum. This setup not only facilitates the transition of the Adam phase from divergence to convergence(Zhang et al., 2022b; Reddi et al., 2019) but also allows a larger β_2 to enhance long-term memory, smoothing the training process and helping to prevent issues like gradient instability. However, as NN parameters scale up, LLMs now use a β_2 value of 0.95 instead of the previous 0.999.

Even when addressing instability in the training process of large models by tuning β_2 , potential spikes in the training trajectory may still occur, where a fixed β_2 can cause the adaptive ratio,

$$r_t = \frac{m_t}{\sqrt{v_t}} \quad (9)$$

to shift from a unimodal distribution approaching zero gradient to a bimodal one, which may destabilize LLM training.

In other words, fixing β_2 establishes a range within which gradient fluctuations remain manageable, especially avoiding sharp increases. Otherwise, a slow EMA could introduce bias in the adaptive coefficient, ultimately harming model performance.(Molybog et al., 2023; Takase et al., 2023)

This study addresses the challenge associated with the β_2 coefficient by introducing a dynamic β_2 that adjusts according to the current training state, enhancing adaptability and stability. The approach leverages the ratio between the current and past squared gradients, allowing sudden gradients to be immediately reflected in v_t and strengthening the convergence stability.

$$\beta_2 \leftarrow 1 - \frac{x_t}{x_{t-1}} |0.5 - P| \quad (10)$$

Notably, in cases where the current-to-past squared gradient ratio exceeds 1, β_2 may even take on negative values, further enhancing adaptability during drastic gradient changes. This mechanism outperforms a simple β_2 setting of zero by providing better adaptive control, as shown in the equation below.

$$v_t = g_t^2 - \beta_2(g_t^2 - v_{t-1}) \quad (11)$$

$$\text{where } \beta_2(g_t^2 - v_{t-1}) > 0 \quad (12)$$

Another critical aspect of our β_2 design is including the P factor, which also serves as an indicator of convergence. When the P factor is near 0, it reveals whether the directions of the gradient and momentum are aligned and provides insight into their relative magnitudes. This makes it a reliable measure of how close the training process is to convergence. Moreover, the reduced β_2 allows the current gradient to contribute more significantly to the second momentum update, giving the algorithm greater “confidence” in its convergence.

When gradients begin to diminish—a phenomenon known as gradient vanishing—the influence of the P factor allows β_2 to approach 1, effectively maintaining long-term memory. This adjustment offers two significant benefits: it enables the model to better handle high-plateau regions, where gradients tend to be low, and it encourages convergence toward flatter minima. Such convergence is beneficial for achieving smoother and potentially more generalizable solutions.

2.3. Acceleration factor ξ

The adaptive coefficient has generally been influenced by both first- and second-order moments. However, alternative methods have been proposed to address challenges such as the risk of convergence to local optima and generalization issues. For instance, the Tiger(Su, 2023) and Lion(Chen et al., 2024) optimizers rely on the sign of the gradient for adaptation, while Adabelief(Zhuang et al., 2020) replaces the squared gradient with the difference between the gradient and momentum. In this study, we tackle similar issues

Algorithm 1 Frankenstein optimizer

Require: learning rate α

initialize $\theta_0, m_0, v_0, t \leftarrow 0, x_0 \leftarrow \alpha, \alpha_0 \leftarrow \alpha$
repeat
 $t \leftarrow t + 1$
 $g_t \leftarrow \nabla_{\theta} f_t(\theta_{t-1})$
 $\beta_{1,t} \leftarrow \text{Clip}(0.1\sqrt{\alpha_t/10^{-3}}, 0.05, 0.99)$
 $P \leftarrow \cos^{-1}(\tanh(m_{t-1} \odot g_t))/\pi$
 $x_t \leftarrow g_t^2 + \epsilon, v_t \leftarrow \max(v_{t-1}, x_t)$
 $\rho \leftarrow \log(\text{Clip}((e^1 + \sqrt{x_t} + 0.5 - P), e^{0.8}, e^{1.05}))$
 $\xi \leftarrow (1 + e^{-0.5})/(1 + e^{-|x_{t-1} - P|})$
 $m_t \leftarrow \rho \beta_{1,t} m_{t-1} - \alpha_t g_t \xi / \sqrt{v_t}$
 $\theta_t \leftarrow \theta_{t-1} + \beta_{1,t} m_t - \alpha_t g_t \xi / \sqrt{v_t}$
 $\beta_{2,t} \leftarrow 1 - \frac{x_t}{x_{t-1}} |0.5 - P|$
 $v_t \leftarrow \beta_{2,t} v_t + (1 - \beta_{2,t}) x_t$
until θ_t converged

by introducing an additional parameter(Dubey et al., 2019), ξ , which is estimated using the following equation.

$$\xi \leftarrow \frac{1 + e^{-0.5}}{1 + e^{-|x_{t-1} - P|}} \quad (13)$$

The parameter ξ is computed based on the final difference between the squared gradient’s magnitude and the P factor (the Non-linear Transformation of the dot product of the gradient and momentum). This estimation helps determine whether convergence has been reached and whether to adjust the learning rate accordingly. In the example shown in Fig.1, the gradients exhibit periodic and dramatic changes, which often cause most optimizers to get trapped in a local optimum due to rapidly diminishing gradient values.

However, the term $|x_{t-1} - P|$ enables the process to be dominated by x_{t-1} under normal conditions, while the P factor takes precedence during rapid gradient changes. This mechanism reduces the risk of converging to a local minimum. As depicted in the figure, the Frankenstein adaptive factor demonstrates a recurring pattern, with the P factor dominating ξ during an “idling phase” until a significant gradient change occurs.

For a more precise characterization of the optimizer’s behavior, Table 1 documents its performance metrics and the dynamics of primary update parameters across successive training stages (Early Training, Mid-Training, Near Convergence) and in extreme cases (Gradient Spikes; Vanishing Gradients).

Table 1. Summary of conditions: behavior of ρ based on gradient square x_t , factor P and β_2 .

Condition	x_t	P	$\rho\beta_1$	β_2	Optimizer Implication
Early Training	Large	~ 0	Large (~ 0.95)	~ 0.5	SGD with high momentum
Mid-Training	Moderate	Increasing	Decreasing	Increasing	Adam with low β_2
Near Convergence	Small	~ 0.5	~ 0.9	high β_2	Adam with high β_2
Gradient Spike	Very large	> 0.5	< 0.9	very low β_2	SGD with low momentum
Vanishing Gradients	Very Small	> 0.5	~ 0.9	≈ 1	Adam with ultra high β_2

 Table 2. Validation Top-1 error rate on ImageNet-1K classification. *(Zhuang et al., 2020), +(Chen et al., 2018), \oplus (Xie et al., 2024)

Optimizer	ResNet18	ResNet50
Adam (Kingma, 2014)	33.46*	23.10 \oplus
Lookahead-Adam (Zhang et al., 2019)	-	24.51
Radam (Liu et al., 2019)	32.38*	-
AMSGrad (Reddi et al., 2019)	32.31+	-
Adabound (Luo et al., 2019)	31.87*	-
PAAdam (Chen et al., 2018)	29.93+	-
AdaBelief (Zhuang et al., 2020)	29.92*	-
SGD (Robbins & Monro, 1951)	29.77*	23.00 \oplus
LAMB (You et al., 2019)	31.36 \oplus	23.00 \oplus
AdaFisher (Martins Gomes et al., 2024)	-	22.99
Adan (Xie et al., 2024)	29.10 \oplus	21.90\oplus
Frankenstein -40 epoch (Ours)	31.24	25.5
Frankenstein -80 epoch (Ours)	29.13	22.9
Frankenstein -120 epoch (Ours)	28.75	22.44

3. Experimental results

3.1. Image classification

3.1.1. LEARNING FROM SCRATCH

We assessed the performance using the ImageNet-1K(Russakovsky et al., 2015) dataset. With the timm(Wightman, 2019) framework, we trained both ResNet18 and ResNet50(He et al., 2016) models, repeating the training process five times. Given that many studies evaluating optimizers compare ImageNet training over 200 epochs, it is impressive that Frankenstein achieves comparable results to Adam in just 40 epochs, as shown in Table 2. It is also comparable to state-of-the-art optimizers like Adan and AdaFisher in just 80 epochs in ResNet18 model architecture.

3.1.2. FINE-TUNING

Transfer learning across different domains has become a widely adopted approach in deep learning. In this study, we trained various optimizers on EfficientNet architectures ranging from B0 to B6, fine-tuning parameters originally learned from ImageNet-1K on the CIFAR-100 dataset. We reconfigured the initial classifier with a MLP layer to align with the target number of classes. Notably, we applied

full parameter fine-tuning throughout to achieve optimal performance. Frankenstein got the best accuracy for B1, B2, B5, and B6 while providing the fastest convergence as shown in Fig.2.

3.2. Language modeling

3.2.1. NATURAL LANGUAGE UNDERSTANDING

The experiment used the IMDB movie review dataset(Maas et al., 2011) to fine-tune a BERT(Devlin, 2018) model for binary sentiment classification. Two GRU(Chung et al., 2014) layers were integrated after the transformer(Vaswani, 2017) architecture to perform the final classification.

The dataset was divided into training, validation, and test sets, with 30% of the data allocated for validation and the remaining 70% for training. The test set was kept separate and used solely for performance evaluation. All optimizers were tested under consistent hyperparameters to ensure fair comparison. Specifically, a learning rate of 2×10^{-4} and a batch size of 128 were applied across all models, with training conducted over 50 epochs. Frankenstein also achieved the fastest convergence among its competitors, as well as superior generalization, as shown in Fig. 3.

3.2.2. NATURAL LANGUAGE GENERATION

The instruction fine-tuning of the LLaMA-7B(Touvron et al., 2023) using Parameter-Efficient Fine-Tuning (PEFT)(Mangrulkar et al., 2022) will serve as a benchmark test. LoRA(Hu et al., 2021) is integrated by adding branches with rank dimension 8 to each layer's `q_proj` and `v_proj` modules. The Alpaca dataset(Taori et al., 2023), generated via self-instruct(Wang et al., 2022) from `text-davinci-003`, used while 2,000 samples reserved for the test. The model is trained with a batch size of 120 for 3 epochs with a cosine annealing schedule, and the performance is evaluated using maximum token lengths of 256 and 512. As shown in Fig.4, Sophia achieves lower training loss than Frankenstein but worse test loss, indicating overfitting. In addition, the Adam optimizer is affected by grouping sequences based on their length during training, which results in performance spikes on the test set. This behavior reflects an underlying issue of training instability.

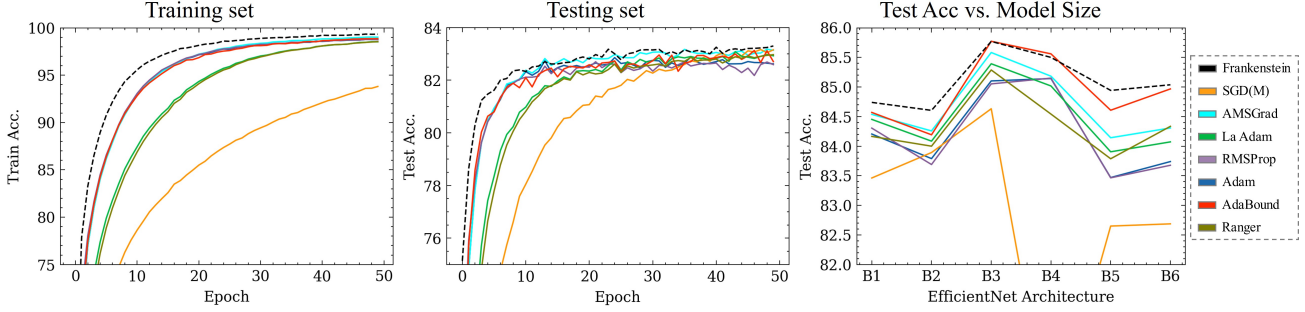


Figure 2. Testing set accuracy profiles of various optimizers on EfficientNetB0 with CIFAR-100 (a) and (b). (c) Testing set accuracy according to architectures (EfficientNetB0-6).

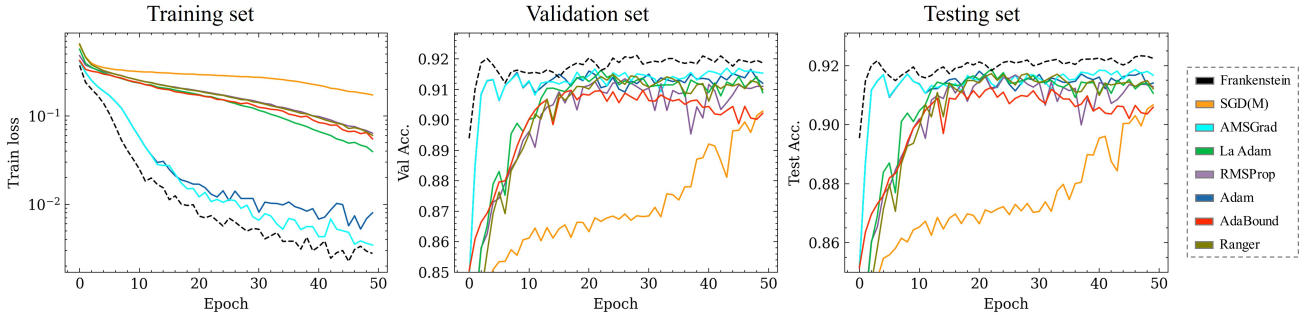


Figure 3. Training, validation and testing set accuracy with different optimizers deal with IMDB movie reviews using BERT.

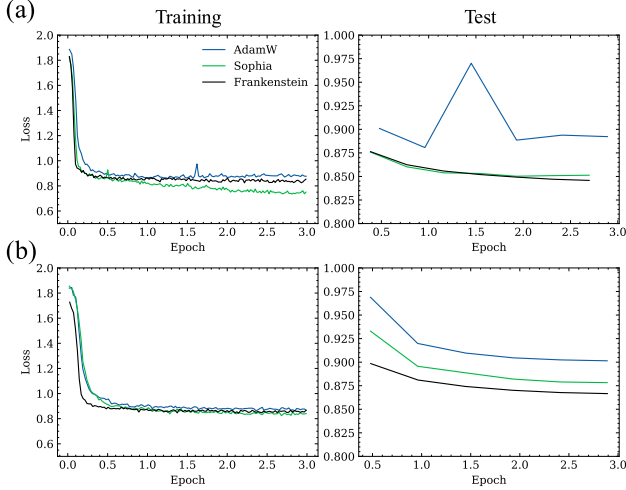


Figure 4. Training and testing losses for text lengths (a) 256 and (b) 512 from the instruction-tuning process of the LLaMA 7B model.

3.3. Few-shot learning

This experiment uses MAML (Model-Agnostic Meta-Learning)(Finn et al., 2017; Antoniou et al., 2018; Li et al., 2017), a framework involving a two-stage optimization process, as a performance benchmark. During the few-shot learning process, MAML undergoes meta-training across

multiple classification tasks, allowing the model to learn generalizable features and effectively initialize its parameters. MAML can quickly adapt to Omniglot(Lake et al., 2013) classification tasks with high accuracy, even with only a few update steps and a minimal number of samples. The learning process uses an optimizer in the inner loop to adjust the model based on transferable data, while an optimizer in the outer loop evaluates the model's overall learning effectiveness. This setup allows us to observe the learning dynamics of different algorithms. For simplicity, gradient descent is used as the update method for the inner loop. The experiments were conducted under 5-way and 20-way settings with 5-shot conditions. Frankenstein exhibits faster convergence and higher accuracy than others (Fig.5).

3.4. Material modeling and simulations

Gradient-based optimization plays a crucial role in scientific simulations as well as deep learning, closely linked to simulation accuracy.

3.4.1. ENERGY MINIMIZATION

In energy minimization experiments, it is necessary to minimize both the atomic position to reduce corresponding potential energy and ensure that the model is reasonable at the start of the simulation. This process involves multiple itera-

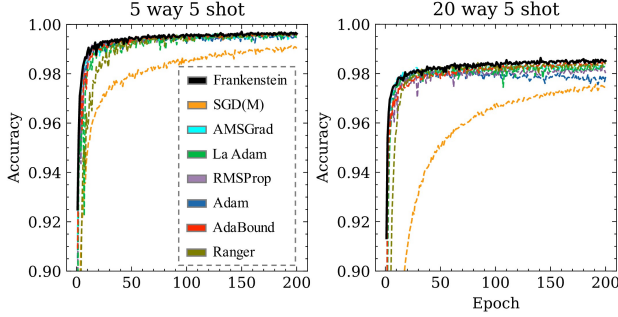


Figure 5. The testing result of several optimizers on the Model-Agnostic Meta-Learning task with multiple strategies.

tions until the energy converges. The classic Lennard-Jones potential problem with 38 atoms is demonstrated during the study. The experiment involves randomly initializing 1,000 structures and testing for convergence when the total force drops to the 1×10^{-2} level. By analyzing the average, minimum, and maximum number of steps required by common algorithms, the differences between algorithms in molecular dynamics during energy minimization are highlighted. The entire energy minimization process is performed with Atomic Simulation Environment (ASE)(Larsen et al., 2017) framework, with all initial atomic structures sourced from Lennard-Jones 38 of OptBench(Centennial). In this benchmark, the number of force calls needed to reach the global minimum is recorded. Frankenstein reaches the global minimum with the least average steps as shown in Table 3. However, the maximum step count is relatively high, possibly due to the different structure of the energy landscape compared to that with flat minima in deep learning.

Table 3. Minimization Benchmarks on Lennard-Jones 38 Clusters

Algorithm	\bar{N}	Min N	Max N
Steepest Descent	4901	1355	9982
BFGS	463	243	8210
Conjugate Gradient	453	207	1153
Fire	656	208	1000
Frankenstein	383	183	3469

To investigate the case of more complex structures, a polycrystalline high-entropy alloy (HEA) model composed of Co, Ni, Cr, Fe, and Mn is generated using Atomsk(Hirel, 2015). The energy minimization of the entire system uses the Second Nearest-Neighbor Modified Embedded-Atom Method (2NN MEAM)(Lee & Baskes, 2000; Hsieh et al., 2020) potential. The system consists of 5.5 million atoms forming a periodic box with $40 \times 40 \times 40$ nm dimensions. All optimization processes are performed using LAMMPS(Thompson et al., 2022), and the minimization methods are executed according to recommended param-

Table 4. Energy minimization on polycrystal high entropy alloy

Method	Error PE (eV)↓	Dislocation segments↓	Dislocation length (nm)↓
Frankenstein	0	8406	7775
Fire	1172	8627	8369
CG	1216	9469	9328
HFTN	1358	8853	8426

eters. Three commonly used optimization methods are adopted as references: FIRE(Guénolé et al., 2020), conjugate gradient (CG), and the Hessian-free truncated Newton algorithm(HFTN). Notably, the best-observed value so far is considered the minimum due to the absence of a well-defined global minimum energy value. Compared to widely used competitors, Frankenstein effectively escapes local optima and reaches the lowest energy state (Fig.6).

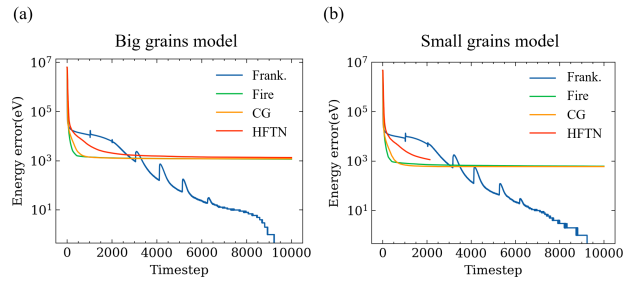


Figure 6. The optimization benchmark for the energy minimization algorithm applied to polycrystal high-entropy alloys according to the grain size. The values indicate the difference between the potential energy of the entire system and the best result found to date (i.e., the result achieved by the Frankenstein search).

Additionally, the system's microstructural analysis after energy minimization is performed using dislocation analysis(Stukowski et al., 2012) (Table 4). The atomic model optimized by our algorithm approaches the accurate minimum potential energy and achieves a significant reduction in the total length and the number of dislocations. This enhanced stability of our Frankenstein suggests that future experiments will be less prone to biases arising from initialization-related defects.

3.4.2. COLLABORATION WITH MATERIALS DISCOVERY

Matbench Discovery(Riebesell et al., 2024) is introduced as a framework to support various NN potentials for assessing the accuracy of predictions of solid-state thermodynamic stability. MACE(Batavia et al., 2023), as a pre-trained foundation model for potentials, is incorporated and benchmarked alongside various energy minimization methods. During the process, models are capped at a maximum of 500 iterations or a force threshold below 1×10^{-2} as the stopping criterion. The experiment applies relaxation to the initial structures

Table 5. Matbench Discovery Benchmarks on MACE

	LBFGS	FIRE	Frankenstein
Error > 1ev/atom (count)	1229	1076	1034
MAE (meV)	97.64	96.3	95.64

of 257k inorganic crystals from the WBM dataset (Wang et al., 2021). Two key indicators are used to evaluate the optimization methods: the number of systems with an energy error > 1 eV/atom (indicating convergence failure) and the average energy error after filtering. Frankenstein fails the least and, on average, reaches a lower energy state as shown in Table 5.

3.4.3. NEURAL NETWORK QUANTUM STATE

In this experiment, we construct a 2D quantum spin lattice model H_{J_1, J_2} with nearest-neighbor (J_1) and next-nearest-neighbor (J_2) interactions, where the coupling constants are set to fully frustrated (Choo et al., 2019) as $J_1 = 1$ and $J_2 = 0.5$, which likely indicate to have numerical sign problem for the neural network quantum state (Szabó & Castelnovo, 2020). The Hamiltonian is generated using the Pauli representation and converted into a sparse matrix format for computational efficiency. We then calculate the eigenvalues using the neural network quantum state $|V_{nn}\rangle$ to estimate the ground state energy $\frac{\langle V_{nn} | H_{J_1, J_2} | V_{nn} \rangle}{\langle V_{nn} | V_{nn} \rangle}$, providing an indicator of the system's stability. A NN, composed of layered linear and ReLU activations, generates a normalized complex parameter vector to optimize the initial quantum states. Each optimizer undergoes 32 convergence tests to ensure stability and consistency. The model's performance is evaluated by minimizing energy discrepancies, offering insights into optimizing quantum states for hybrid quantum-classical computing (Zhang et al., 2022a) and materials simulations (Yoshioka et al., 2021). The landscape of NNQS is notorious to train, but Frankenstein achieves the lowest loss frequently, as shown in Fig. 7.

4. Analysis

We examined the changes in NN weights and representations during training, focusing on their impact on generalization and the learning process (Li et al., 2018). To visualize the weights of the entire network (EfficientNetB0, which contains 5.3 million parameters) in a 2D space, the weights at each training epoch were recorded and reduced to two dimensions using PCA. The produced network-specific hyperplane encapsulates the optimizer's training trajectory. Based on the PCA1 and PCA2 coordinates of each point in this space, the model's weights were reconstructed, and performance was evaluated on the CIFAR-100 testing set.

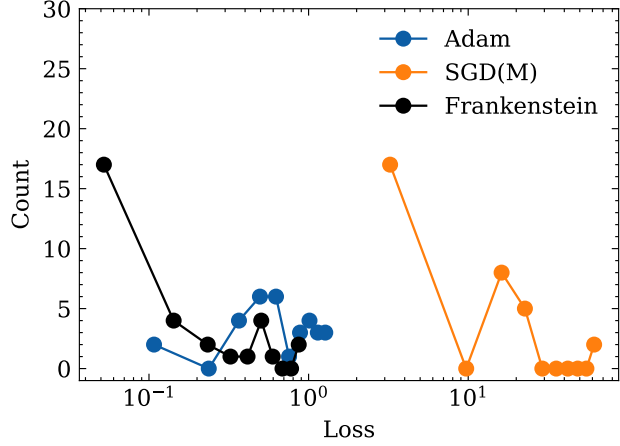


Figure 7. Distribution of loss after 10k iterations for different optimizers over 32 tests of simulating a quantum system with neural network training to approximate the lowest energy eigenstate of a Hamiltonian.

The training trajectory is illustrated on the plane using black arrows. This hyperplane reveals distinct preferences for different optimizers, as shown in Fig. 8. For instance, Adam tends to overfit, as it quickly deviates from the flat minima region. In contrast, our Frankenstein exhibits a stabilized trajectory in a landscape with superior generalization after reaching the target region.

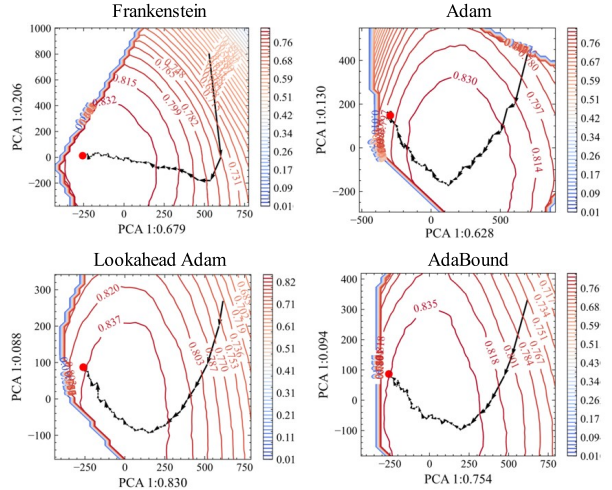


Figure 8. The learning process of different optimizers during transfer learning on EfficientNetB0 using the CIFAR-100 dataset. The contour lines represent the model's accuracy on the test set.

In addition to analyzing NN weights, examining changes in NN representations is a valuable approach to understanding how low-level features propagate through layers and transform into high-level semantics. The Centered Kernel Alignment (CKA) method (Kornblith et al., 2019; Davari

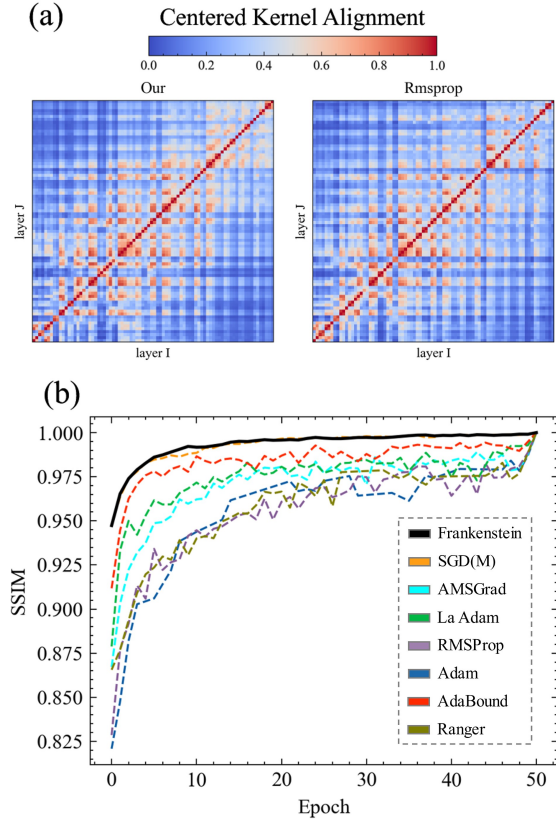


Figure 9. (a) Centered kernel alignment (CKA) show the difference of representations between RmsProp and Frankenstein. (b) History profiles of structural similarity index between different epoch and 50th epoch CKA matrix, to define the effective forming period of the functional network.

et al., 2022; Muttenhaler et al., 2024) has been proposed as an effective tool for addressing such problems, as it highlights representation changes across different architectures. By approximating an identity matrix, where the information between layers becomes maximally decorrelated, each layer sufficiently transforms the information and reveals the influence of architecture on model representations.

In this study, we present the results of CKA analysis in Fig. 9(a), comparing the performance of RMSprop with our proposed algorithm. The results clearly show that our method effectively prevents low-level features from leaking into layers near the output. Addit in fine-tuned models, a cross-optimizer analysis is shown in Fig. 9(b), where CKA maps from each epoch are compared to the final converged result. Matrix similarity is measured using the Structural Similarity Index (SSIM) metric. It is important to note that while task performance metrics such as loss and accuracy can be clearly quantified, they do not adequately capture whether the learned representations undergo substantial changes during fine-tuning. This aspect is crucial for understanding

the model's zero-shot capability. To investigate this, we use representations pre-trained on large-scale datasets, such as ImageNet, as a strong baseline and then apply simple fine-tuning on a downstream task, such as CIFAR-100. If the model weights remain largely unchanged while still achieving strong performance on the downstream task, this suggests that the representations are stable. This stability can be assessed by measuring the CKA similarity between the final model and the initial pre-trained model. A higher similarity indicates minimal representational drift. In our experiments, we observed that models more prone to overfitting, such as those trained with Adam or RMSProp, showed greater divergence in their final representations

5. Conclusion

In this paper, we proposed the Frankenstein optimizer, dynamically adjusting its momentum coefficients to improve convergence. We comprehensively evaluated our Frankenstein to demonstrate its versatility and effectiveness across broad applications. It offers superiority in complex deep learning tasks such as image classification, instruction fine-tuning, sentiment classification, and collaborative optimization for meta-learning. It also has potential to advance materials design by treating challenges such as structural optimization, energy minimization, and defect reduction. In quantum applications, our optimizer efficiently navigated the ‘barren plateau’ while others didn’t. Additionally, our analyses using CKA and the loss landscape visualization provided deeper insights into the behavior of adaptive optimizers during training. Overall, the Frankenstein optimizer has demonstrated its ability to tackle impactful problems in AI, science, and engineering, paving the way for breakthroughs across multiple domains.

Impact Statement

Recently, many advances in science and engineering have increasingly relied on machine learning methods to tackle existing challenges. Our algorithm, applicable for any gradient-based trainable model, is designed to improve computational efficiency, robust generalization, and adaptability across diverse tasks. Our research has the potential to be applied to various technologies, including the superintelligence, material and drug design, and quantum security. However, we believe that it is not necessary to specifically discuss their social and ethical implications at this stage.

This study also emphasizes the recombination of various findings, showcasing how rational integration of multiple prior improvements can enhance performance. The CKA and landscape methods serve as valuable tools for analyzing learning dynamics, providing insights into the behavior of both optimizers and models. During this process, we ob-

served that certain popular algorithms enjoy a privileged (Elhage et al., 2023) status across different fields. Furthermore, the values of our momentum coefficients, β and β_2 , remain within the range of 0 to 1. As a result, we did not perform a formal convergence analysis.

Acknowledgments

This work was supported by SES AI. Computational resources were partially provided by the Texas Advanced Computing Center (TACC) and the MIT SuperCloud. Additional support was provided by the “High Entropy Materials Center,” funded through the Featured Areas Research Center Program under the Higher Education Sprout Project by the Ministry of Education (MOE), Taiwan.

References

Abadi, M., Barham, P., Chen, J., Chen, Z., Davis, A., Dean, J., Devin, M., Ghemawat, S., Irving, G., Isard, M., et al. {TensorFlow}: a system for {Large-Scale} machine learning. In *12th USENIX symposium on operating systems design and implementation (OSDI 16)*, pp. 265–283, 2016.

Adler, B., Agarwal, N., Aithal, A., Anh, D. H., Bhattacharya, P., Brundyn, A., Casper, J., Catanzaro, B., Clay, S., Cohen, J., et al. Nemotron-4 340b technical report. *arXiv preprint arXiv:2406.11704*, 2024.

Antoniou, A., Edwards, H., and Storkey, A. How to train your maml. In *International conference on learning representations*, 2018.

Batatia, I., Benner, P., Chiang, Y., Elena, A. M., Kovács, D. P., Riebesell, J., Advincula, X. R., Asta, M., Avaylon, M., Baldwin, W. J., et al. A foundation model for atomistic materials chemistry. *arXiv preprint arXiv:2401.00096*, 2023.

Brown, T., Mann, B., Ryder, N., Subbiah, M., Kaplan, J. D., Dhariwal, P., Neelakantan, A., Shyam, P., Sastry, G., Askell, A., et al. Language models are few-shot learners. *Advances in neural information processing systems*, 33: 1877–1901, 2020.

Centennial, G. W. W. Minimization benchmarks for lennard-jones 38 clusters. URL <https://theory.cm.utexas.edu/benchmarks/minimization.html#lj38>.

Chen, J., Zhou, D., Tang, Y., Yang, Z., Cao, Y., and Gu, Q. Closing the generalization gap of adaptive gradient methods in training deep neural networks. *arXiv preprint arXiv:1806.06763*, 2018.

Chen, X., Liang, C., Huang, D., Real, E., Wang, K., Pham, H., Dong, X., Luong, T., Hsieh, C.-J., Lu, Y., et al. Symbolic discovery of optimization algorithms. *Advances in neural information processing systems*, 36, 2024.

Choo, K., Neupert, T., and Carleo, G. Two-dimensional frustrated j 1-j 2 model studied with neural network quantum states. *Physical Review B*, 100(12):125124, 2019.

Chung, J., Gulcehre, C., Cho, K., and Bengio, Y. Empirical evaluation of gated recurrent neural networks on sequence modeling. *arXiv preprint arXiv:1412.3555*, 2014.

Davari, M., Horoi, S., Natik, A., Lajoie, G., Wolf, G., and Belilovsky, E. Reliability of cka as a similarity measure in deep learning. *arXiv preprint arXiv:2210.16156*, 2022.

Devlin, J. Bert: Pre-training of deep bidirectional transformers for language understanding. *arXiv preprint arXiv:1810.04805*, 2018.

Dubey, A., Jauhri, A., Pandey, A., Kadian, A., Al-Dahle, A., Letman, A., Mathur, A., Schelten, A., Yang, A., Fan, A., et al. The llama 3 herd of models. *arXiv preprint arXiv:2407.21783*, 2024.

Dubey, S. R., Chakraborty, S., Roy, S. K., Mukherjee, S., Singh, S. K., and Chaudhuri, B. B. diffgrad: an optimization method for convolutional neural networks. *IEEE transactions on neural networks and learning systems*, 31(11):4500–4511, 2019.

Elhage, N., Lasenby, R., and Olah, C. Privileged bases in the transformer residual stream. *Transformer Circuits Thread*, pp. 24, 2023.

Finn, C., Abbeel, P., and Levine, S. Model-agnostic meta-learning for fast adaptation of deep networks. In *International conference on machine learning*, pp. 1126–1135. PMLR, 2017.

Goyal, P., Dollár, P., Girshick, R., Noordhuis, P., Wesolowski, L., Kyrola, A., Tulloch, A., Jia, Y., and He, K. Accurate, large minibatch sgd: Training imagenet in 1 hour. arxiv 2017. *arXiv preprint arXiv:1706.02677*, 2019.

Guénolé, J., Nöhring, W. G., Vaid, A., Houllé, F., Xie, Z., Prakash, A., and Bitzek, E. Assessment and optimization of the fast inertial relaxation engine (fire) for energy minimization in atomistic simulations and its implementation in lammps. *Computational Materials Science*, 175: 109584, 2020.

He, K., Zhang, X., Ren, S., and Sun, J. Deep residual learning for image recognition. In *Proceedings of the IEEE conference on computer vision and pattern recognition*, pp. 770–778, 2016.

Hirel, P. Atomsk: A tool for manipulating and converting atomic data files. *Computer Physics Communications*, 197:212–219, 2015.

Hsieh, K.-T., Lin, Y.-Y., Lu, C.-H., Yang, J.-R., Liaw, P. K., and Kuo, C.-L. Atomistic simulations of the face-centered-cubic-to-hexagonal-close-packed phase transformation in the equiatomic co-crfe-mnni high entropy alloy under high compression. *Computational Materials Science*, 184:109864, 2020.

Hu, E. J., Shen, Y., Wallis, P., Allen-Zhu, Z., Li, Y., Wang, S., Wang, L., and Chen, W. Lora: Low-rank adaptation of large language models. *arXiv preprint arXiv:2106.09685*, 2021.

Kingma, D. P. Adam: A method for stochastic optimization. *arXiv preprint arXiv:1412.6980*, 2014.

Kornblith, S., Norouzi, M., Lee, H., and Hinton, G. Similarity of neural network representations revisited. In *International conference on machine learning*, pp. 3519–3529. PMLR, 2019.

Lake, B. M., Salakhutdinov, R. R., and Tenenbaum, J. One-shot learning by inverting a compositional causal process. *Advances in neural information processing systems*, 26, 2013.

Larsen, A. H., Mortensen, J. J., Blomqvist, J., Castelli, I. E., Christensen, R., Dułak, M., Friis, J., Groves, M. N., Hammer, B., Hargus, C., et al. The atomic simulation environment—a python library for working with atoms. *Journal of Physics: Condensed Matter*, 29(27):273002, 2017.

Lee, B.-J. and Baskes, M. I. Second nearest-neighbor modified embedded-atom-method potential. *Physical Review B*, 62(13):8564, 2000.

Li, H., Xu, Z., Taylor, G., Studer, C., and Goldstein, T. Visualizing the loss landscape of neural nets. *Advances in neural information processing systems*, 31, 2018.

Li, Z., Zhou, F., Chen, F., and Li, H. Meta-sgd: Learning to learn quickly for few-shot learning. arxiv 2017. *arXiv preprint arXiv:1707.09835*, 2017.

Liu, A., Feng, B., Xue, B., Wang, B., Wu, B., Lu, C., Zhao, C., Deng, C., Zhang, C., Ruan, C., et al. Deepseek-v3 technical report. *arXiv preprint arXiv:2412.19437*, 2024.

Liu, H., Li, Z., Hall, D., Liang, P., and Ma, T. Sophia: A scalable stochastic second-order optimizer for language model pre-training. *arXiv preprint arXiv:2305.14342*, 2023.

Liu, L., Jiang, H., He, P., Chen, W., Liu, X., Gao, J., and Han, J. On the variance of the adaptive learning rate and beyond. arxiv 2019. *arXiv preprint arXiv:1908.03265*, 2019.

Luo, L., Xiong, Y., Liu, Y., and Sun, X. Adaptive gradient methods with dynamic bound of learning rate. *arXiv preprint arXiv:1902.09843*, 2019.

Lyu, K. and Li, J. Gradient descent maximizes the margin of homogeneous neural networks. *arXiv preprint arXiv:1906.05890*, 2019.

Maas, A., Daly, R. E., Pham, P. T., Huang, D., Ng, A. Y., and Potts, C. Learning word vectors for sentiment analysis. In *Proceedings of the 49th annual meeting of the association for computational linguistics: Human language technologies*, pp. 142–150, 2011.

Mangrulkar, S., Gugger, S., Debut, L., Belkada, Y., Paul, S., and Bossan, B. Peft: State-of-the-art parameter-efficient fine-tuning methods. <https://github.com/huggingface/peft>, 2022.

Martins Gomes, D., Zhang, Y., Belilovsky, E., Wolf, G., and Hosseini, M. S. Adafisher: Adaptive second order optimization via fisher information. *arXiv e-prints*, pp. arXiv–2405, 2024.

McClean, J. R., Boixo, S., Smelyanskiy, V. N., Babbush, R., and Neven, H. Barren plateaus in quantum neural network training landscapes. *Nature communications*, 9(1):4812, 2018.

Molybog, I., Albert, P., Chen, M., DeVito, Z., Esiobu, D., Goyal, N., Koura, P. S., Narang, S., Poulton, A., Silva, R., et al. A theory on adam instability in large-scale machine learning. *arXiv preprint arXiv:2304.09871*, 2023.

Muttenhaler, L., Linhardt, L., Dippel, J., Vandermeulen, R. A., Hermann, K., Lampinen, A., and Kornblith, S. Improving neural network representations using human similarity judgments. *Advances in Neural Information Processing Systems*, 36, 2024.

Reddi, S. J., Kale, S., and Kumar, S. On the convergence of adam and beyond. *arXiv preprint arXiv:1904.09237*, 2019.

Riebesell, J., Goodall, R., Benner, P., Chiang, Y., Deng, B., Lee, A., Jain, A., and Persson, K. Matbench discovery—a framework to evaluate machine learning crystal stability predictions, 2024. *arXiv preprint arXiv:2308.14920*, 2024.

Robbins, H. and Monro, S. A stochastic approximation method. *The annals of mathematical statistics*, pp. 400–407, 1951.

Russakovsky, O., Deng, J., Su, H., Krause, J., Satheesh, S., Ma, S., Huang, Z., Karpathy, A., Khosla, A., Bernstein, M., et al. Imagenet large scale visual recognition challenge. *International journal of computer vision*, 115: 211–252, 2015.

Smith, S. Don’t decay the learning rate, increase the batch size. *arXiv preprint arXiv:1711.00489*, 2017.

Stukowski, A., Bulatov, V. V., and Arsenlis, A. Automated identification and indexing of dislocations in crystal interfaces. *Modelling and Simulation in Materials Science and Engineering*, 20(8):085007, 2012.

Su, J. Tiger: A tight-fisted optimizer. <https://github.com/bojone/tiger>, 2023.

Szabó, A. and Castelnovo, C. Neural network wave functions and the sign problem. *Physical Review Research*, 2 (3):033075, 2020.

Takase, S., Kiyono, S., Kobayashi, S., and Suzuki, J. Spike no more: Stabilizing the pre-training of large language models. *arXiv preprint arXiv:2312.16903*, 2023.

Taori, R., Gulrajani, I., Zhang, T., Dubois, Y., Li, X., Guestrin, C., Liang, P., and Hashimoto, T. B. Stanford alpaca: An instruction-following llama model, 2023.

Thompson, A. P., Aktulga, H. M., Berger, R., Bolintineanu, D. S., Brown, W. M., Crozier, P. S., In't Veld, P. J., Kohlmeyer, A., Moore, S. G., Nguyen, T. D., et al. Lammmps-a flexible simulation tool for particle-based materials modeling at the atomic, meso, and continuum scales. *Computer Physics Communications*, 271:108171, 2022.

Tieleman, T. Lecture 6.5-rmsprop: Divide the gradient by a running average of its recent magnitude. *COURSERA: Neural networks for machine learning*, 4(2):26, 2012.

Touvron, H., Lavigil, T., Izacard, G., Martinet, X., Lachaux, M.-A., Lacroix, T., Rozière, B., Goyal, N., Hambro, E., Azhar, F., et al. Llama: Open and efficient foundation language models. *arXiv preprint arXiv:2302.13971*, 2023.

Vaswani, A. Attention is all you need. *Advances in Neural Information Processing Systems*, 2017.

Villalobos, P., Sevilla, J., Besiroglu, T., Heim, L., Ho, A., and Hobbahn, M. Machine learning model sizes and the parameter gap. *arXiv preprint arXiv:2207.02852*, 2022.

Wang, H.-C., Botti, S., and Marques, M. A. Predicting stable crystalline compounds using chemical similarity. *npj Computational Materials*, 7(1):12, 2021.

Wang, Y., Kordi, Y., Mishra, S., Liu, A., Smith, N. A., Khashabi, D., and Hajishirzi, H. Self-instruct: Aligning language models with self-generated instructions. *arXiv preprint arXiv:2212.10560*, 2022.

Wightman, R. Pytorch image models. <https://github.com/rwightman/pytorch-image-models>, 2019.

Wilson, A. C., Roelofs, R., Stern, M., Srebro, N., and Recht, B. The marginal value of adaptive gradient methods in machine learning. *Advances in neural information processing systems*, 30, 2017.

Wright, L. and Demeure, N. Ranger21: a synergistic deep learning optimizer. *arXiv preprint arXiv:2106.13731*, 2021.

Wu, K., Zhang, J., Peng, H., Liu, M., Xiao, B., Fu, J., and Yuan, L. Tinyvit: Fast pretraining distillation for small vision transformers. In *European conference on computer vision*, pp. 68–85. Springer, 2022.

Wu, X., Ward, R., and Bottou, L. Wngrad: Learn the learning rate in gradient descent. *arXiv preprint arXiv:1803.02865*, 2018.

Xie, X., Zhou, P., Li, H., Lin, Z., and Yan, S. Adan: Adaptive nesterov momentum algorithm for faster optimizing deep models. *IEEE Transactions on Pattern Analysis and Machine Intelligence*, 2024.

Yoshioka, N., Mizukami, W., and Nori, F. Solving quasiparticle band spectra of real solids using neural-network quantum states. *Communications Physics*, 4(1):106, 2021.

You, Y., Li, J., Reddi, S., Hseu, J., Kumar, S., Bhojanapalli, S., Song, X., Demmel, J., Keutzer, K., and Hsieh, C.-J. Large batch optimization for deep learning: Training bert in 76 minutes. *arXiv preprint arXiv:1904.00962*, 2019.

Zhang, M., Lucas, J., Ba, J., and Hinton, G. E. Lookahead optimizer: k steps forward, 1 step back. *Advances in neural information processing systems*, 32, 2019.

Zhang, S.-X., Wan, Z.-Q., Lee, C.-K., Hsieh, C.-Y., Zhang, S., and Yao, H. Variational quantum-neural hybrid eigensolver. *Physical Review Letters*, 128(12):120502, 2022a.

Zhang, Y., Chen, C., Shi, N., Sun, R., and Luo, Z.-Q. Adam can converge without any modification on update rules. *Advances in neural information processing systems*, 35: 28386–28399, 2022b.

Zhou, P., Feng, J., Ma, C., Xiong, C., Hoi, S. C. H., et al. Towards theoretically understanding why sgd generalizes better than adam in deep learning. *Advances in Neural Information Processing Systems*, 33:21285–21296, 2020.

Zhuang, J., Tang, T., Ding, Y., Tatikonda, S. C., Dvornek, N., Papademetris, X., and Duncan, J. Adabelief optimizer: Adapting stepsizes by the belief in observed gradients. *Advances in neural information processing systems*, 33: 18795–18806, 2020.

A. More experiment detail

Regarding the from-scratch training results on ImageNet, as shown in the figure below, we ran experiments using ResNet-18 and ResNet-50 for 120 epochs. Each experiment was repeated 5 times, and only the average values are reported in the fig 10. The hyperparameters were adopted from the recommended settings in the TIMM library(Wightman, 2019). For example, for ResNet-18, we used: `--batch-size 256 (across 4 GPUs)`, `--weight-decay 1e-2`, `--sched step`, `--lr 1e-3`, `--epochs 120`, `--min-lr 1e-5`, `--decay-epochs 40`, `--amp`. No specific hyperparameter search was performed, and the batch size was limited by the GTX 2080Ti 11 GB VRAM. Additionally, we examined the training behavior of Tiny ViT(Wu et al., 2022) with various optimizers, as shown in Fig. 11.

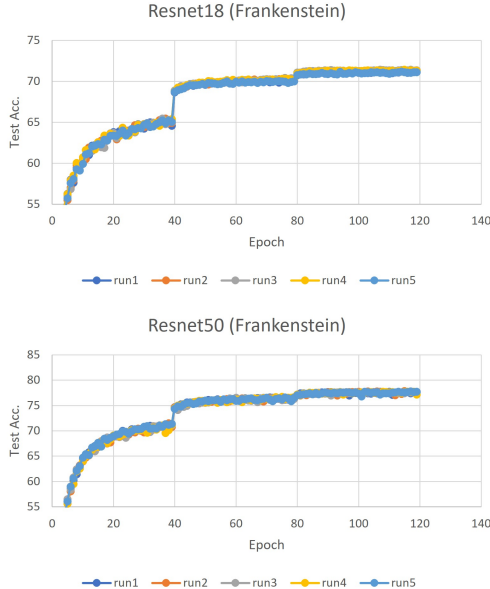


Figure 10. Test accuracy progression during training for Resnet18 and Resnet50 Frankenstein optimizer. The curves represent multiple independent runs, illustrating training stability and convergence.

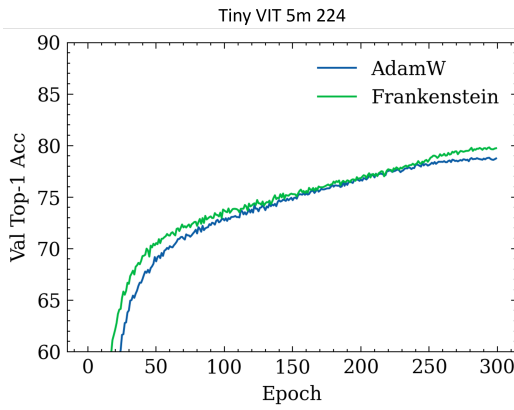


Figure 11. Validation Top-1 Accuracy of Tiny ViT 5m 224 on ImageNet. Comparing performance with AdamW and Frankenstein optimizers.

B. Hyperparameter

In our experiments, we conducted a comprehensive evaluation of various optimization algorithms, ranging from classical momentum-based methods to modern adaptive and state-of-the-art optimizers. We assessed their performance across standard tasks like image classification (on CIFAR-10/100) and natural language processing (using BERT fine-tuning), as well as on challenging scenarios such as few-shot learning. To gain deeper insights into optimizer behavior, we employed techniques including the visualization of the loss landscape as a probe and the analysis of neural network representation similarity.

To address concerns regarding experimental reproducibility and provide robust results, all experiments were conducted with five independent runs. The final performance metrics presented are the average results across these repeated trials to ensure reliability.

While adaptive optimizers generally offer greater robustness to hyperparameter choices, we performed systematic tuning for all optimizers on each task to ensure fair comparisons and report results based on their best achievable performance.

For the CIFAR-10/100 and NLU tasks, we conducted a hyperparameter search to identify the optimal settings for each optimizer. Tables 6 and 7 detail the learning rate search spaces explored. Other hyper-parameters, such as weight decay, were kept consistent across optimizers where applicable, or tuned individually when necessary for optimal performance.

Table 6. Hyper-parameters searching for NLU tasks.

Learning rate	Batch size
5×10^{-4}	128
1×10^{-4}	
5×10^{-5}	
If using SGD, lr $\times 10$	

Table 7. Hyper-parameters searching for Cifar tasks.

Learning rate	Batch size
5×10^{-3}	128
1×10^{-3}	512
5×10^{-4}	
1×10^{-4}	
If using SGD, lr $\times 10$	

C. Update rule comparison of various optimizers

Several adaptations have been developed for various optimizers, each addressing specific characteristics. These improvements include:

- Adding momentum and implementing a bias correction mechanism (Adam([Kingma, 2014](#))).
- Resolving EMA's non-convergence issues by adopting a more rigorous approach (AMSGrad([Reddi et al., 2019](#))).
- Introducing constraints on the adaptive range to enhance stability (Adabound([Luo et al., 2019](#))).
- Allowing for control over adaptation across different powers, enabling adjustable adaptive rates (Padam([Chen et al., 2018](#))).
- Using the difference between the current gradient and momentum as an adaptive component(Adabelief([Zhuang et al., 2020](#))).

Table 8. Update rules of various optimizers

Algorithm	Update Rule
RMSProp(Tieleman, 2012)	$v_t \leftarrow \beta_2 v_{t-1} + (1 - \beta_2) g_t^2$
Adam(Kingma, 2014)	$v_t \leftarrow \frac{\beta_2 v_{t-1} + (1 - \beta_2) g_t^2}{1 - \beta_2^t}$
AmsGrad(Reddi et al., 2019)	$v_t \leftarrow \max \left(\frac{\beta_2 v_{t-1} + (1 - \beta_2) g_t^2}{1 - \beta_2^t}, v_{\max} \right)$
Adabound(Luo et al., 2019)	$v_t \leftarrow \text{Clip} \left(\beta_2 v_{t-1} + (1 - \beta_2) g_t^2, v_{\min}, v_{\max} \right) t$
Padam(Chen et al., 2018)	$v_t \leftarrow \max \left(\frac{\beta_2 v_{t-1} + (1 - \beta_2) g_t^2}{1 - \beta_2^t}, v_{t-1} \right)^{2p}$
Adabelief(Zhuang et al., 2020)	$v_t \leftarrow \frac{\beta_2 v_{t-1} + (1 - \beta_2) (g_t - m_t)^2}{1 - \beta^t}$
Frankenstein (Ours)	$v_t \leftarrow \beta_2 v_{t-1} + (1 - \beta_2) g_t^2,$ where $\beta_2 = 1 - \frac{g_t^2}{g_{t-1}^2} 0.5 - P $ where $P \leftarrow \cos^{-1}(\tanh(m_{t-1} \odot g_t)) / \pi$

D. Ablation experiments

To demonstrate the role of each component in the optimizer, we conducted ablation experiments on an image classification task. Specifically, we trained the EfficientNet-B0 model (initialized randomly) on the CIFAR-10 dataset and used the final testing accuracy as a metric to evaluate the impact on performance. The training process utilized a batch size of 128 and a learning rate of 1×10^{-3} for 100 epochs, reducing the learning rate by a factor of 10 every 40 epochs.

The experiments involved modifications to the momentum settings (e.g., decoupling β from the learning rate and fixing $\beta = 0.9$) and second-order momentum terms (e.g., removing v_t , fixing $\beta_2 = 0.999$, excluding $\max(v_{t-1}, x_t)$, and omitting the EMA of v_t). In total, six variations were analyzed to assess their effect on performance using the test set.

Table 9. Ablation experiments: The ablation study was tested on the CIFAR-10 dataset, with the neural network architecture being EfficientNetB0. Results are the average of 5 experimental runs.

Case	Test set Accuracy
Full	93.17 ± 0.17
Fix $\beta_2 = 0.999$	92.32 ± 0.29 (-0.85)
Decouple β with LR	92.22 ± 0.22 (-0.95)
Adam	92.12 ± 0.17 (-1.05)
Fix $\beta = 0.9$	92.08 ± 0.28 (-1.09)
w/o $\max(v_{t-1}, x_t)$	91.77 ± 0.87 (-1.4)
w/o EMA of v_t	91.74 ± 0.42 (-1.43)

As shown in the table 9, the performance of each variation is compared with the original algorithm. Notably, when the dynamically adjusted first-order and second-order momentum coefficients (β and β_2) are fixed to constant values—similar to Adam optimizer default parameters—the convergence results are almost equivalent to Adam optimizer final performance.

E. Adaptive overfit test

To evaluate whether these adaptive hypotheses introduce additional biases (e.g., bias correction from Adam(Kingma, 2014), Radam’s variance control policy(Liu et al., 2019)) that could lead to overfitting, we introduce a simple binary classification task(Wilson et al., 2017). The inputs and classifications for this task are defined by the following equation:

for $i = 1, \dots, n$, where $n = 6$.

$$x_{ij} = \begin{cases} y_i & j = 1, \\ 1 & j = 2, 3, \\ 1 & j = 4 + 5(i-1), \dots, 4 + 5(i-1) + 2(1-y_i), \\ 0 & \text{otherwise,} \end{cases}$$

In this experiment, we tested two different batch sizes (4 and 128) to explore the relationship between adaptivity and noise(Zhou et al., 2020), as illustrated in Fig. 12. Nearly all optimizers achieved extremely low training loss (10^{-9}), which was limited by precision constraints. Notably, AMSGrad, due to its strategy of maximizing v_t at each step, struggled to adapt to this type of problem. On the test set (depicted on the right side of the figure), our proposed algorithm demonstrated robust convergence across various conditions, particularly when compared to other adaptive optimizers.

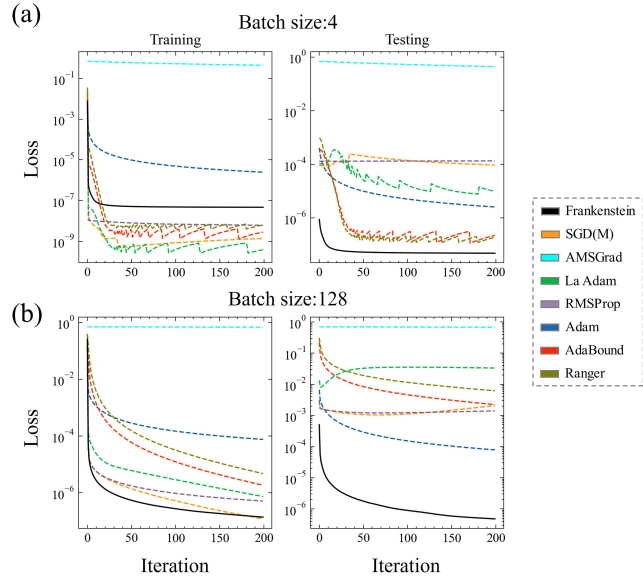


Figure 12. Demonstrate the overfitting behavior of various adaptive algorithms when applied to simple problems, with batch sizes of 4 and 128 shown in (a) and (b), respectively.

F. Loss landscape for energy minimization

The loss landscape for visualizing high-dimensional spaces has also been applied to the analysis of the energy minimization process in polycrystalline high-entropy alloys using molecular dynamics models. We compared the behavior of our algorithm with the Conjugate Gradient method on the energy landscape, as illustrated in Fig. 13. The acceleration effect achieved by our adaptive approach is clearly demonstrated in the contour plots and learning trajectories, showcasing an optimization process that follows the steepest and most efficient path.

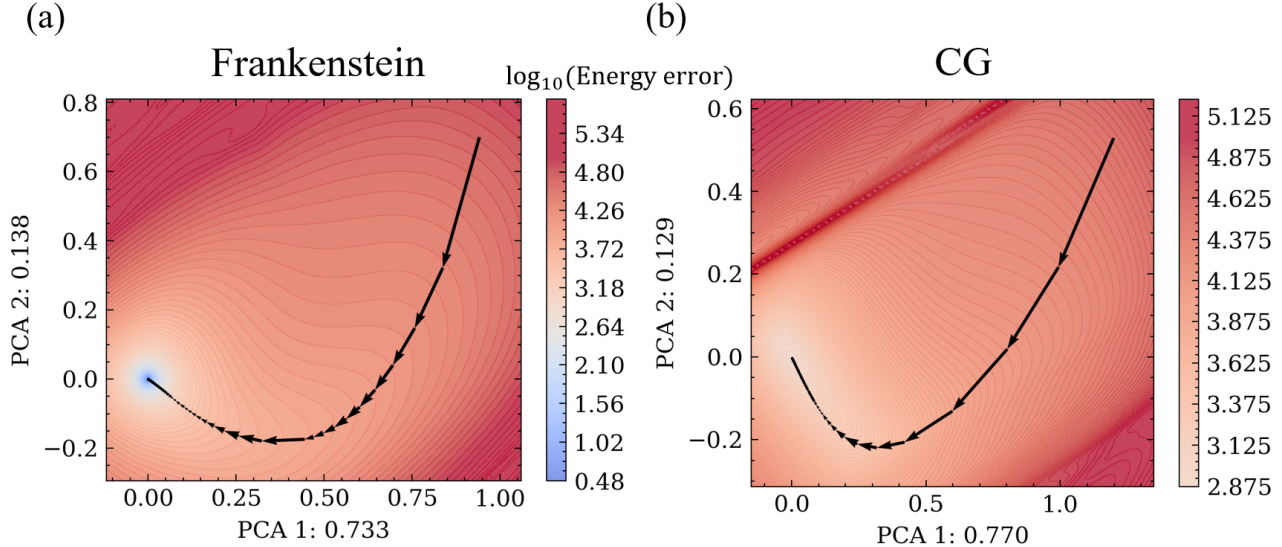


Figure 13. Illustrate the energy minimization process for (a) Frankenstein and (b) CG on polycrystalline high-entropy alloys. The contour lines indicate the difference between the potential energy of the entire system and the best result obtained thus far.

G. Optimizer setting

SGD(M): Whether the momentum parameter is case sensitive, we implement the most commonly applied value of 0.9. Additionally, the momentum behavior was fellow the Nesterov Accelerated Gradient (NAG), which has more solid theoretical converge guarantees.

RmsProp([Tieleman, 2012](#)): In the experiment, the adaptive learning optimizer would take into account being a competitor. RmsProp adjusts the learning rate of each weight with the magnitudes of gradients. Following TensorFlow instruction, we set a smoothing constant with a default value of 0.9.

Adam([Kingma, 2014](#)) & Amsgrad([Reddi et al., 2019](#)): Adam is the most commonly used optimizer, which interjects the bias correction mechanism that significantly helps the initial few training steps. Furthermore, Adam's variant, i.e., AMSGrad, facilitates the problem that can't converge. We set the β_1 and β_2 as 0.9, 0.999, respectively.

Lookahead([Zhang et al., 2019](#)): Lookahead optimizer is independent of these previous optimizers, which be aid of optimizer. In the experiment, it supports Adam optimizer that parameter set as we mention above. Then, the Lookahead mechanism would manipulate as five sync periods and having 0.5 slow step size.

Adabound([Luo et al., 2019](#)): Adabound is a variant of Adam, that dynamic bounds on elements learning rate. Therefore, it enables the training processing with Adam-like initial and SGD-like eventually. We apply the default setting on experiments, i.e., the final learning ratio is 0.1.

Ranger([Wright & Demeure, 2021](#)): Ranger is the combination of Lookahead and Rectified Adam. Note that it is regarded as the state-of-the-art optimizer, which can achieve the best performance on a worldwide task. As an influential competitor, we set the suggestion hyperparameter by TensorFlow([Abadi et al., 2016](#)).